Pure appl. geophys. 164 (2007) 1–24
DOI 10.1007/s00024-007-0253-0

Pure and Applied Geophysics

Effects of Drying on the Low-Frequency Electrical Properties of Tournemire Argillites

Philippe Cosenza,[1] Ahmad Ghorbani,[1] Nicolas Florsch,[1] and André Revil[2]

Abstract—Nearly water-saturated argillite samples (initial water content near 3.4 wt%) were cored from an undisturbed area of an underground facility of the French Institute for Radioprotection and Nuclear Safety (IRSN), located at Tournemire (Aveyron, France). These samples were subjected to the following desiccation path: (a) A desaturation phase during which the samples were dried at ambient temperature conditions, relative humidity equal to 43% in average and (b) a heating phase during which the same samples were heated at four temperature levels from 70°C up to 105°C. During both phases, the low-frequency complex resistivity (0.18Hz–12 kHz) was recorded by a four-electrode device.The amplitude of the complex resistivity was extremely sensitive to water content change. At the end of the isotherm desaturation phase, it was multiplied by a factor of 3 to 5. During the heating phase, the resistivity increased by more than two orders of magnitude compared to the initial state. The percentage of Frequency Effect shows a low sensitivity to water content changes during the desaturation stage while it increased by two orders of magnitude during the heating phase. This result confirms that low-frequency spectral signature is extremely sensitive to textural changes (i.e., thermal-induced microcracking in this case) that occurred during heating. Moreover, the complex resistivity of the samples shows a strong anisotropy (a ratio of 10 between both amplitudes measured in the perpendicular directions). The classical Cole-Cole model cannot be used to fit the experimental data obtained in the heating phase. A generalized formulation of this model is required and was successfully applied to represent the complex resistivity data.

Key words: Spectral-induced polarization, complex resistivity, argillite, drying, microcracks.

1. Introduction

In many industrial countries (such as Belgium, Germany, France, Japan, Spain, Switzerland) deep argillaceous formations are considered as potential host media for high level radioactive wastes. This is because clayey geomaterials have the ability to adsorb a large amount of ions and they possess the low permeability required to slow down the percolations of fluids (e.g., Mitchell, 1973). In France, in order to

[1] Université Pierre et Marie Curie, UMR Sisyphe, Case 105 - Tour 46/56- 3ème étage 4, place Jussieu, 75252, Paris Cedex 05, France. E-mail: cosenza@ccr.jussieu.fr
[2] UMR 6635, CNRS-CEREGE, Université d'Aix-Marseille III, Aix-en-Provence, France.

S B 0 1 0 2 5 3 B
Journal number | Manuscript number
Dispatch: 1.6.2007 Journal: Pure and applied Geophysics No. of pages: 24
Author's disk received ☑ Used ☑ Corrupted ☐ Mismatch ☐ Keyed ☐

improve the knowledge of the containment properties of such formations, two geological sites are currently under study: the Callovo-Oxfordian argillites of the Paris Basin (e.g., ANDRA, 2005a) and the Toarcian argillites of Tournemire, in the Southern France (e.g., CABRERA *et al.*, 2001).

For the safety assessment of long-term radioactive waste disposals, a critical issue is the impact of the thermo-hydro-mechanical loading induced by the excavation of deep galleries and by the exothermic canisters (e.g., KALUZNY, 1990; ANDRA, 2005b). In this framework, it is desirable to have non-invasive tools in order to determine *in situ* petrophysical parameters (like the porosity, the permeability, the water content) and the textural changes that can be induced by thermal and mechanically induced cracking during the construction and the life of the underground repository.

Complex resistivity method also named Spectral Induced Polarization (SIP) consists of measuring both the low-frequency resistivity and the phase shift between the voltage and the applied current. This is a very promising geophysical method to monitor both water content and fracturing of argillaceous rocks. Indeed, low-frequency and DC resistivity are often used to determine the water content of porous materials (e.g., DANNOWSKI and YARAMANCI, 1999), and electrical spectroscopy can be used as an efficient tool to detect fractures (GLOVER *et al.*, 1997, 2000; NOVER *et al.*, 2000; HEIKAMP and NOVER, 2003). Moreover, recent *in situ* investigations in the Mont Terri underground laboratory (KRUSCHWITZ and YARAMANCI, 2004) showed that SIP can be qualitatively used to characterize the so-called "excavation damaged zone" (EDZ) located around the galleries. The EDZ is generated by the excavation because of the stress and temperature changes and the desiccation of argillites.

Nevertheless, to our knowledge, no extensive experimental SIP investigation has been performed on argillaceous rocks with a high clay content (typically greater than 30 wt%) in the low-frequency range, typically 10 mHz to 10 kHz. In our opinion, this is mainly due to two reasons. On the one hand, for a long time the oil and mineral companies were not interested in investigating the physical properties of shale. On the other hand, SIP measurements in the low-frequency range (typically less than 10 Hz), are difficult to conduct since they require the removal of the spurious electrode polarizations occurring at the boundary between the sample and the measuring electrodes (e.g., VINEGAR and WAXMAN, 1984; GARROUCH and SHARMA, 1994; LEVITSKAYA and STENBERG, 1996; CARRIER and SOGA, 1999; CHÉLIDZE *et al.*, 1999). The substitution technique based on electrolytic cells between the sample and the current electrodes (e.g., VINEGAR and WAXMAN, 1984; OLHOEFT, 1985) cannot be used for argillaceous rock as their texture is extremely sensitive to water content and salinity changes. Moreover, the use of rigid and "nonpolarizing" electrodes with a platinum coating requires an extremely good sample to electrode contact in order to minimize the corresponding contact resistance. This contact may be difficult to get and it is wellknown that black

platinum electrodes are brittle and easily damaged when clamped against rock samples (see LEVITSKAYA and STENBERG, 1996).

This is why the first goal of this study is to establish a simple and reliable procedure in order to measure low-frequency complex electrical resistivity of an argillaceous rock. The second goal of our study in relation to the monitoring of underground facilities, is to assess the ability of SIP to measure both water content changes and fracturing. In this purpose, the desiccation path is preferred, starting with samples close to saturation, cored in the undisturbed zone of the site. The third objective of our paper concerns the quantitative modelling of the experimental data. We examine below the simplest models describing the effects of desiccation on the measured low-frequency electrical properties of the argillites.

2. Geological Overview and Sampling Strategy

The site of Tournemire was chosen as a test site by the French Institute for Radioprotection and Nuclear Safety (IRSN) to study the confining properties of argillites for research purposes. This site is located in southern France, in the western border of the Causses Basin, a Mesozoic sedimentary basin. The general stratigraphy of the Tournemire massif is subhorizontal (Fig. 1A.). Three major formations are identified. The lower formations (Hettangian, Sinemurian and Carixian) and the upper formations (Upper Aalenian, Bajocian and Bathonian) consist of limestones and dolomites. The intermediate formations (Domerian and Toarcian) correspond to marls and argillaceous rocks. The main geological target of the studies conducted by IRSN is the upper Toarcian formation corresponding to a layer 160 m thick of argillites.

The Toarcian formation is intercepted by a set of boreholes and two galleries drilled from an old railway tunnel crossing the Upper Toarcian (CABRERA *et al.*, 2001) (Fig. 1A.). The mineralogical composition of samples taken from boreholes shows that clay minerals (kaolonite, illite, and interstratified illite-smectite) represent about 40 wt.% of the bulk-rock composition (DE WINDT *et al.* 1998; CHARPENTIER *et al.*, 2004). The coarse fraction contains quartz ($\sim$ 20 wt.%), K-feldspars, bioclasts, and pyrite ($\sim$ 2 wt.%). Carbonates (calcite with minor dolomite and siderite) constitute 15 wt.% of the bulk-rock composition. Geochemical studies (e.g., BONIN, 1998; DE WINDT *et al.* 1998) and mechanical investigations (e.g., NIANDOU *et al.*, 1997; COSENZA *et al.*, 2002) confirmed that Tournemire argillite consists of transverse isotropic material. Some physico-chemical properties of Tournemireargillites are given in Table 1.

A set of four samples was taken from the boreholes TM90 and TM180 (Fig. 1B.), which were drilled in 2005 perpendicular to the wall of the main tunnel. The TM90 borehole is subhorizontal and parallel to the bedding in the Toarcian formation and TM180 was drilled vertically in the same formation perpendicular to the tunnel axis. This configuration allows investigatation of the degree of anisotropy of this material. The drilling was carried out with air to avoid contact of the formation with any kind

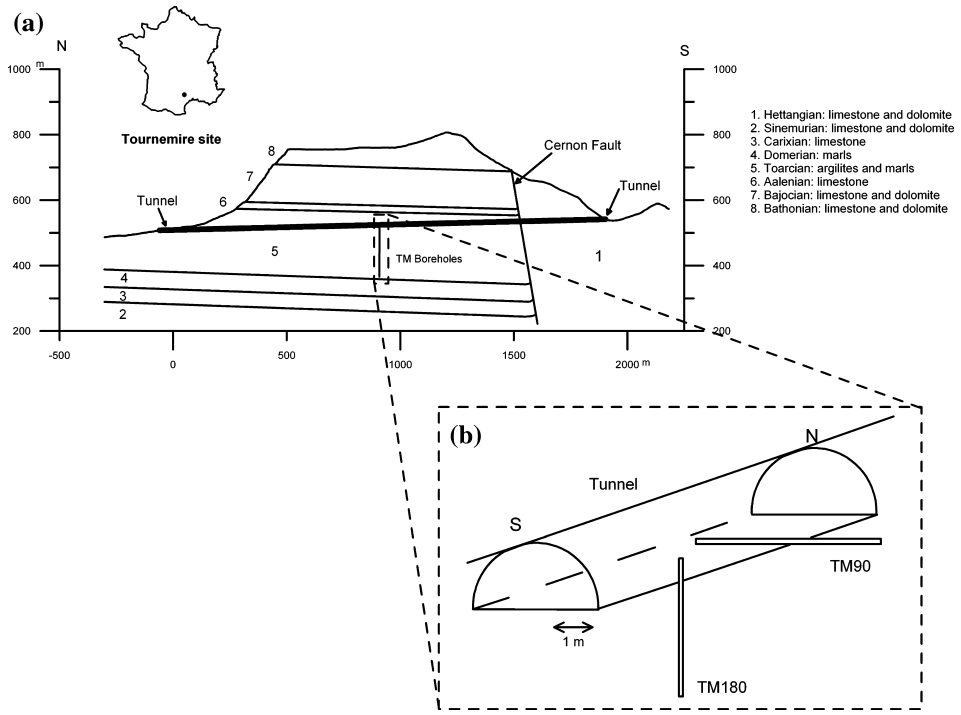

Figure 1
(a) Geological cross section of the Tournemire tunnel (modified from CABRERA *et al.*, 2001). The tunnel is drawn in bold line; the transversal galleries and all the previous boreholes are not shown. (b) Locations of the TM90 borehole and TM180 borehole (not to scale).

Table 1

Physico-chemical properties of Tournemire (from BONIN, 1998; CABRERA et al., 2001)

Density	2.5–2.6 10^3kg.m^{-3}
Grain density	2.7–2.8 10^3kg.m^{-3}
Pore size	centred around 2.5 nm
Porosity	6–9%
Gravimetric water content	3.5–4%
Specific surface area	23–29 m^2/g
Cation exchange capacity	9.5–10.8 meq/100 g
Hydraulic permeability	10^{-14}–10^{-15} m/s (laboratory)
	10^{-11}–10^{-14} m/s (*in situ*)

of aqueous solutions. Samples were immediately taken after the completion of drilling and put in Al-coated plastic bags under confined N_2 atmosphere. The samples were located between 12 and 14 meters from the gallery wall in a preserved zone outside the so-called Excavation Disturbed Zone (EDZ) and outside the influence of the ambient air. The samples have been cored far from the wall of the

tunnel wall in order to study near-saturated and undamaged argillite samples. This state corresponds therefore to an initial reference state (IRS). In a first stage, in order to understand separately the impact of water content changes and fracturing, it was easier to work with this IRS and not to mix the effects of various (hydraulical and mechanical) processes existing in a material located in the EDZ.

The geometrical features of the samples and their water content are given in Table 2. The low values of water content (3.33 wt.% in average) are typical of this argillite in a natural state (BONIN, 1998). From the variation ranges of the porosity and the grain density given in Table 2, we checked that this average corresponds to a near-saturated state, between 90% and 100% of saturation degree.

3. Methodology

3.1. Experimental Set-up

The SIP FUCHS-II measure the complex resistivity over seven decades of frequency (1.4 mHz up to 12 kHz). It comprises in two remote units that record the current I and voltage U signals (Fig. 2).

The complex impedance Z^* is defined by (e.g., PELTON *et al.*, 1983):

$$Z^*(\omega) = \frac{U}{I} = |Z^*(\omega)|e^{i\,\phi(\omega)}, \tag{1}$$

where $(\mathrm{i}^2 = -1); |Z^*(\omega)|$ and $\phi(\omega)$ are the impedance amplitude and the phase, respectively. They are *a priori* functions of the angular frequency ω. The existence of the phase $\phi(\omega)$ results from polarization processes occurring in the sample, i.e., the so-called Induced Polarization (IP) effect.

To measure the entire spectrum, the SIP FUCHS-II apparatus starts with the highest frequency, 12 kHz, and the N other decreasing frequencies are obtained by the following division: $12\,\mathrm{KHz}/2^{\mathrm{N}}$. Optical fibers are used in order to minimize electromagnetic cross-couplings between the transmitter and the receiver. The measured data are transferred to the base unit, where the apparent resistivity and the phase shift are determined. The SIP FUCHS-II is connected to a computer, to record the data and to display the results in real time.

Table 2

Geometrical features and water content of the samples

Sample	Length (mm)	Diameter (mm)	Water content (wt. %)	Geometrical factor (m)
TM90-1280	193	79.5	3.42	0.0848
TM90-1260	205	79.5	3.33	0.0848
TM180-1424	52.5	79.5	3.49	0.1751
TM180-1288	88	79.5	3.09	0.1731

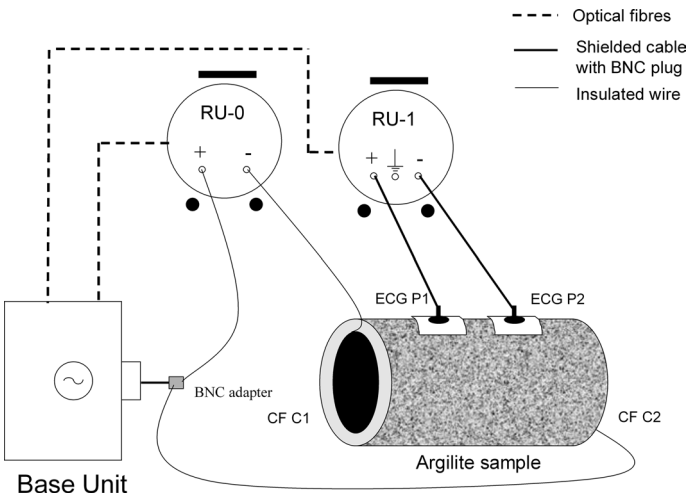

Figure 2
Experimental setup. RU-0: Remote Unit 0 (or Transmitter); RU-1: Remote Unit 1 (or Receiver). Note that both remote units are mobile since SIP-Fuchs II equipment is used for field measurements. ECG P1 and ECG P2: electrocardiogram Ag/AgCl electrodes as potential electrodes; CF C1 and CF C2: Carbon films as current electrodes.

As mentioned, the main difficulty at low frequency is to avoid two spurious effects that interact each other: (a) The disturbing impedance of the electrode-sample contact and (b) the so called ''electrode polarization'' associated with electrochemical reactions occurring at the electrode-sample boundary (e.g., VANHALA and SOININEN, 1995; LEVITSKAYA, and STENBERG, 1996; CHÉLIDZE *et al.*, 1999).

To minimize these effects in simplistically, measurements have been performed with a four-electrode device using low-cost medical electrodes. The potential (or measuring) electrodes and the current (or source) electrodes are electrocardiogram (ECG) Ag/AgCl electrodes (Asept Co.) and thin carbon films (Valutrode® electrodes from Axelgaard Manufacturing Co.), respectively. Silver-silver chloride (Ag/AgCl) electrodes which are known to be stable, almost nonpolarizable in comparison with metal electrodes, are widely used in laboratory SIP measurements (e.g., VINEGAR and WAXMAN, 1984; VANHALA and SOININEN, 1995). In our study, ECGAg/AgCl electrodes consist of a small metal round piece (10 mm diameter) galvanized by silver and covered with a soft sponge imbibed of a AgCl gel. The carbon films (50 mm diameter, 1 mm thick) that are used in electrotherapy are circular and covered with a conductive adhesive gel which provides a good electrical contact between the electrodes and the rock sample (i.e., no air gaps in between).

Our four-electrode device was validated using porous and electrically inert samples. We chose ''clean'' limestone samples. Indeed, ''clean'' (i.e., with no clay fraction) limestone saturated with a highly-conductive brine will not generate

spurious polarization (e.g., VAN VOORHIS *et al.*, 1973; VINEGAR and WAXMAN, 1984). Figure 3 shows the resistivity and the phase spectrum in the range 0.18 Hz–12 kHz of two limestone samples from Lavoux and Vilhonneur. They were characterized by low clay fractions typically less than 1 wt.%, (BEMER *et al.*, 2004) saturated with a 0.1Ω.m brine (NaCl) conductivity. No significant polarization has been measured in the frequency range 0.18 Hz to 12 kHz except for the highest frequency value of 12 kHz for which a small but significant phase shift is observed and likely associated with an electromagnetic coupling/noise effect. The existence of this phase shift implies a small error of about ±1 mrad on the measurements for frequencies greater than 6 kHz. For lower frequencies, the phase shift is less than ±0.5 mrad that is a typical error value for the SIP-Fuchs (e.g., WELLER *et al.*, 1996; BINLEY *et al.*, 2005).

In fact, following the experimental configuration given in Figure 2, and in order to compare the data from the different samples (with different geometries), a geometrical factor K (expressed in meters) has to be calculated in order to convert the measured complex impedance Z^* as complex resistivity ρ^*:

$$\rho^*(\omega) = KZ^*(\omega). \tag{2}$$

The parameter K has been calculated numerically by solving the Laplace equation with a finite-difference scheme. Its value for each sample is given in Table 1. It should be noted that $|\rho^*(\omega)|$ will be called hereafter the amplitude of the complex resistivity.

3.2. Experimental Procedure

The samples were monitored during two phases. In the first phase, called below the "desaturation phase"; the samples were dried at ambient temperature conditions.

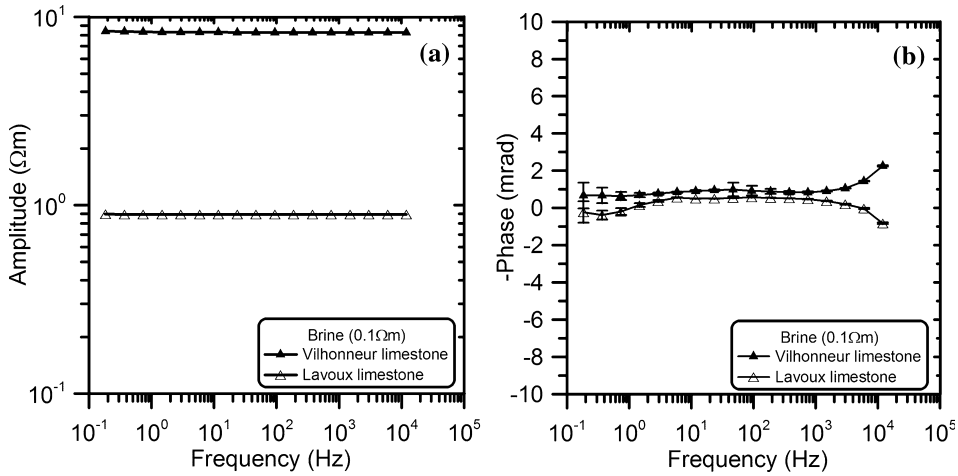

Figure 3
(a) Amplitude spectra of limestone samples. (b) Phase spectra of limestone samples.

In the second phase, called below the ''heating phase'', the same samples were heated at four temperature levels (70, 80, 90 and 105°C).

The desaturation phase provides a desiccation path with samples that are initially nearly water-saturated. It can also mimic the effect of ventilation in an underground gallery. During this phase, different parameters were recorded over time (up to one hour to four days) as a function of the dehydration rate. These parameters are the loss of weight induced by desiccation, the complex resistivity spectrum (phase and amplitude) in the frequency range 0.18 Hz–12 kHz, the relative humidity (RH%), the room temperature and the temperature of the surface of the sample by a noncontact thermometer. The desaturation phase was considered as finished when the sample weights no longer evolved; This phase lasted from 19 to 22 days.

The heating phase was started immediately after the end of the desaturation phase. The same set of samples was subjected to four background temperature levels by an oven: 70°C, 80°C, 90°C, and 105°C. At each level temperature was maintained constant during 24 hours. The last temperature level (105°C) allowed measurement of the initial water content on the basis of the loss of weight of the samples. Before and after each temperature level, the loss of weight and the complex resistivity spectrum were measured. It should be noted that the dielectric spectrum was not recorded immediately after removal from the oven but at least 5 hours afterwards, in order to obtain a thermal equilibrium, i.e., to equilibrate sample temperature and room temperature.

There were several goals that we pursue by doing the measurements during the heating phase. They are (a) to provide physical insights concerning the effect of temperature induced by exothermic nuclear wastes on the dielectric behavior of argillite, (b) to remove a significant part of the ''bound'' water in the microporosity, (c) to generate microcracks in the samples. These microcracks are formed in response to two processes. First, heating is responsible for local thermal stresses in the different components (the different minerals and the interstitial liquid). In turns, these thermal stresses induce local thermal strain incompatibilities and hence microcracks. In addition, the cooling of the samples after their removal from the oven generates a high tensile stress (e.g., BÉREST and WEBER, 1988), which may go beyond the low tensile strength of the argillaceous rock, typically in the range of 2–10 MPa (e.g., ROUSSET, 1988).

4. Results and Qualitative Interpretation

4.1. Loss of Weight under Desiccation

Figures 4a and 4b show the evolution of the water content during both phases (desaturation and heating) for each sample. As mentioned, the duration of the desaturation phase ranged from 19 days (TM90-1260) to 27 days (TM180-1288). The

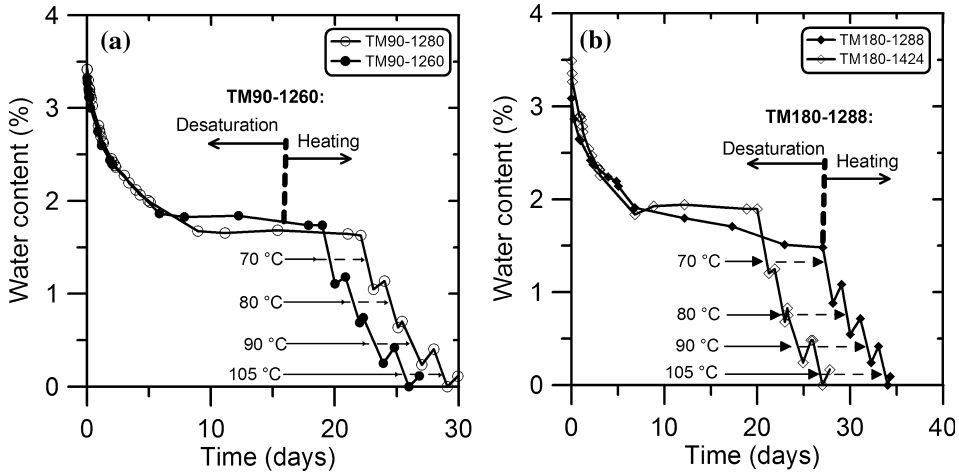

Figure 4
(a) Loss of weight of samples TM90-1260 and TM90-1280 as a function of time. (b) Loss of weight of samples TM180-1424 and TM180-1288 as a function of time.

samples with the same size and from the same borehole (i.e., TM90-1260 and TM90-1280) show similar dehydration rates during the desaturation phase (Fig. 4a). During this phase, the relative humidity was equal to 43% in average. This corresponds to a rather dry atmosphere. Despite this low value of relative humidity, the desaturation induced a limited loss of weight for the whole set of samples. Indeed, they kept half of their initial water content (between 48% and 54%, see Figs. 4a and 4b) at the end of this phase. Consequently, it is suspected that this desaturation phase involved mainly the water removal from the macro and mesoporosity (typically for pore sizes the range 0.8 nm up −50 nm, see for instance ROUQUEROL *et al.*, 1994) and hence moderate textural changes. Indeed, if an adsorbed water layer of thickness d_w surrounding platy particles is considered, the corresponding water content w is proportional to the specific surface S_a, as follows (e.g., MITCHELL, 1993):

$$w = S_a \, d_w \, \rho_w, \tag{3}$$

where ρ_w is water density. By using the approximate equation (3), a mean value of S_a equal to 26 m^2/g, measured by the BET/N_2 method on Tournemire argillite (BONIN, 1998; DEVIVIER *et al.*, 2004) and a value of d_w equal to 0.8 nm (about two diameters of H_2O molecules) give a value of water content associated with microporosity equal to 2.1%. This order of magnitude is confirmed by the results of others experimental studies performed on the same material (VALÈS *et al.*, 2004). Furthermore, it should be emphasized that the water content calculated on the basis of a drying oven at 105°C leads to an underestimate of the real water content in argillite. Indeed, a drying at 105°C during 24 h does not remove all the water, especially "bound" water, in smectite clays (e.g., TESSIER, 1978).

During the heating phase, the small "rebounds" observed in Figures 4a and 4b are related to the removal of the samples from the oven in order to return to a thermal equilibrium with the room.

4.2. Effect of Drying on Amplitude Spectra

Amplitudes obtained during both experimental stages (desaturation and heating phase) at two extreme frequencies (0.18 Hz and 12 kHz) are presented in Figures 5a and 5b as a function of water content.

Considering the desaturation phase, comparatively to the initial near-saturated state, amplitudes of samples TM 90 and TM 180 boreholes were multiplied by a factor of 3 and 5, respectively. This result demonstrates that DC or low-frequency electrical methods are very promising to monitor the evolution of water content. In addition, the anisotropic texture of argillite influences significantly the electrical properties. Indeed, Figures 5a and 5b show that there exists about one order of magnitude between the amplitude parallel to the stratification and that perpendicular to the stratification. Nevertheless, we are aware that this strong contrast may be lower in the field since electrical properties, as for many other physical properties, are stress dependent (e.g., GLOVER *et al.*, 1997). Indeed, the core decompression during the drilling may have induced a small but significant opening of some natural bedding planes in the samples (e.g., NIANDOU *et al.*, 1997).

Moreover, considering the desaturation phase, results show that the relationship between amplitude $|\rho^*|$ and the water content w is slightly frequency-dependent. This result is also illustrated in Figure 6 where the amplitude spectrum of sample TM 90-

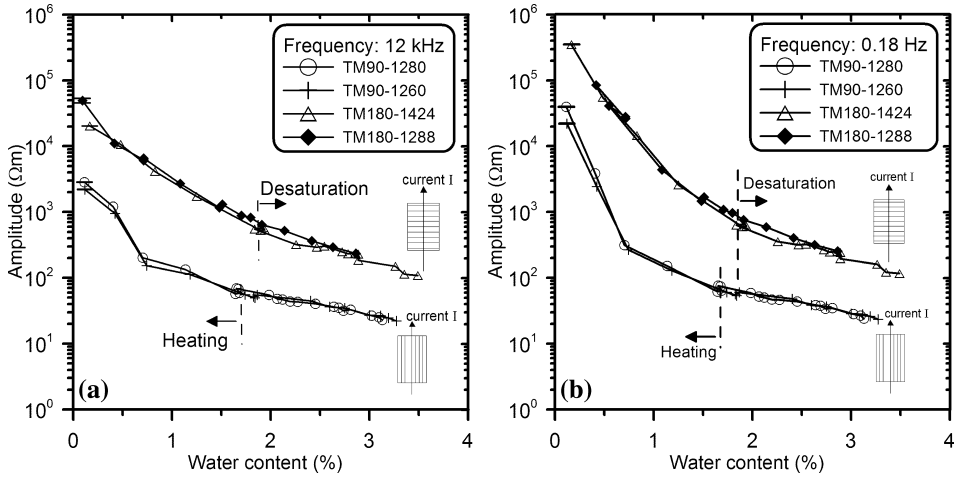

Figure 5

(a) Amplitude at 12 kHz as a function of water content (b) Amplitude at 0.18 Hz as a function of the water content. The direction of the current flow I comparative to the stratification is also shown.

1280 is plotted at different values of water content. On the basis of the discussion given in the previous section, this suggests that the loss of free water from macroporosity does not generate significant distortion of the low-frequency amplitude spectrum. Furthermore, an amplitude spectrum measurement will provide no significant additional insights in regard to *in situ* monitoring of water content.

During the heating phase, the amplitude increases drastically by 2 to 3 orders of magnitude when the background temperature increases. Consequently, the thermal-induced microcracking and the loss of a significant part of "bound" water in the microporosity affect significantly the amplitude spectrum of the complex resistivity (Fig. 6). This can be shown by using the percentage of frequency effect, pFE, (e.g., VAN VOOHRIS *et al.*, 1973)

$$\mathrm{pFE}(\%) = \frac{|\rho^*(0.18\,\mathrm{Hz})| - |\rho^*(12\,\mathrm{kHz})|}{|\rho^*(12\,\mathrm{kHz})|}, \tag{4}$$

where $|\rho^*(0.18\,\mathrm{Hz})|$ and $|\rho^*(12\,\mathrm{kHz})|$ are the amplitudes measured at the two extreme frequencies (0.18 Hz and 12 kHz). The parameter pFE is plotted in Figure 7 as a function of water content. The results illustrate clearly the previous observations given in Figures 5a, 5b, and 6, the pFE remains low and almost constant during the desaturation phase (i.e., no change in amplitude spectrum) while it increases drastically during the heating phase. Consequently, this parameter could be used to discriminate the evolution associated with free water and that with microcracking.

At this stage it is difficult to identify clearly the polarization processes related to the values of pFE measured during the desaturation phase. When clay minerals are

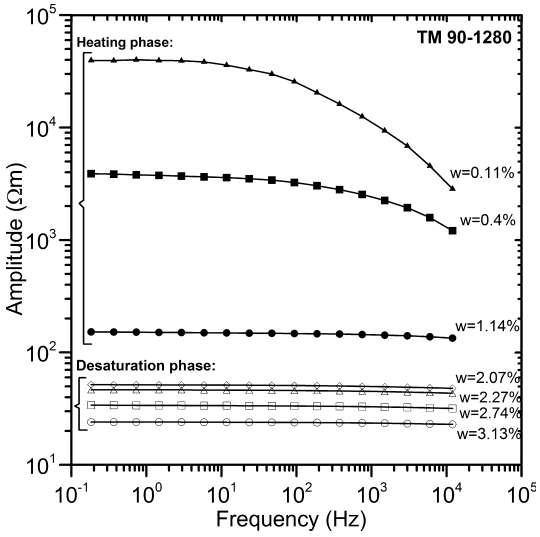

Figure 6
Amplitude spectra of sample TM90-1280 during the desaturation and the heating phase.

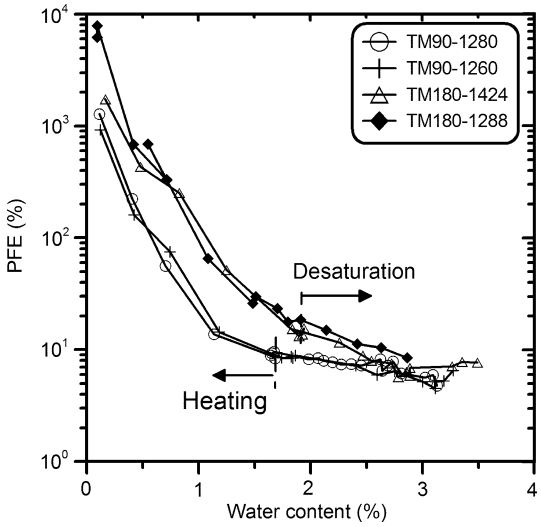

Figure 7
Percentage of Frequency Effect (pFE) as a function of the water content.

present in a sedimentary rock, several researchers have considered that SIP is explained by the "membrane polarization" model, for which the sediment is described by two zones: selective and non-selective domains, which are connected in series (MARSHALL and MADDEN, 1959; KLEIN and SILL, 1982; VINEGAR and WAXMAN, 1984; TITOV *et al.*, 2002). Following this model, the zones are associated with different effective mobilities (or Hittorf transport numbers) of cations and anions which, under the applied external electrical field, produce local charge accumulations and charge density gradients that are responsible for the frequency dependence of the resistivity. However, others polarization processes can be also invoked: the Maxwell-Wagner effect related to the heterogeneity of the material and macroscopic space charge distributions (OLHOEFT, 1985) and the polarization of the electrical double layer (see DUKHIN and SHILOV, 1974; GARROUCH and SHARMA, 1994; VANHALA, 1997; REVIL *et al.*, 1998).

Nevertheless, considering the heating phase associated with much higher values of pFE, the most appealing explanation is to consider the role of the thermal-induced microcracks as micro-capacitors contributing to create displacement currents and hence to induce macroscopically frequency-dependent resistivity measurements. This aspect will be discussed further.

4.3. Effect of Drying on Phase Spectrum

The phase measured during both experimental stages (desaturation and heating phase) at two extreme frequencies (0.18 Hz and 12 kHz) is presented in Figures 8a and 8b as a function of the water content.

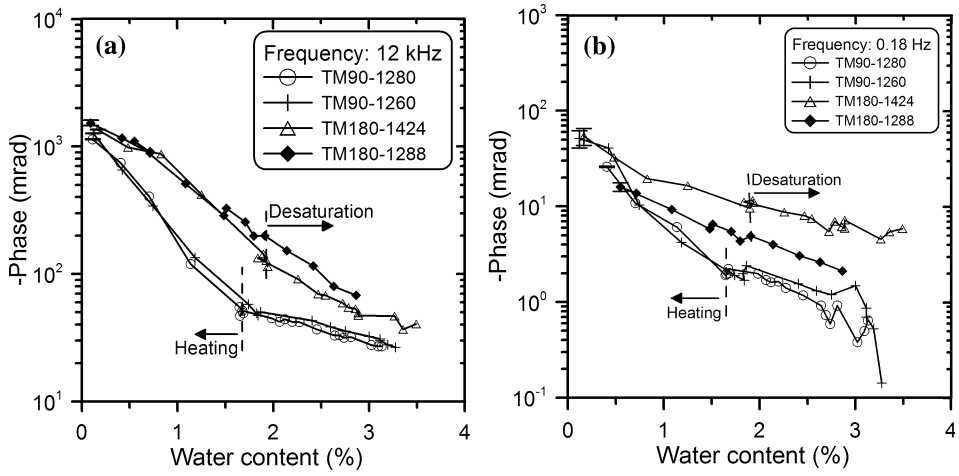

Figure 8
(a) Phase at 12 kHz as a function of water content. (b) Phase at 0.18 Hz as a function of water content. The direction of the current flow I comparative to the stratification is also given.

Contrasting to amplitude measurements, a significant difference in the measured phases between both samples extracted from the same borehole TM180 (called hereafter TM180 samples) can be observed. Since this is not the case for both samples taken from borehole TM90 (horizontally drilled), this difference may be attributed to a slight vertical variation in the mineralogy and/or in the texture. Note that both TM180 samples have different initial water content (Table 1) and are located at 1424 mm and 1288 mm from the gallery wall, respectively.

In comparison with amplitude spectra (Figs. 5a and 5b), Figures 8a and 8b indicate an evolution of the phase over two decades in the whole range of water content values. The phase is less sensitive than amplitude to change in the water content. It should be mentioned that the erratic phase variations for high water content for TM90 samples at 0.18 Hz (Fig. 8b) are due to the measurements of low phase values: these values have the same order of magnitude as the instrumental error.

However, the comparison between the amplitude and phase spectra also evidences similar features. Indeed, both parameters show a continuous evolution with water content for both experimental stages (desaturation and heating) for TM180 samples. Opposite of the TM90 samples, no significant discontinuity in the amplitude and phase can be observed at the desaturation-heating transition. We suggest that this remarkable feature is associated with the anisotropy of the Tournemire argillite. Indeed, the texture of an argillite is characterized by two components (e.g., SAMMARTINO *et al.,* 2003) (Fig. 9A): a coarse and nonconducting phase consisting of grains (mainly tectosilicates and carbonates, in the range of a few dozens up to a

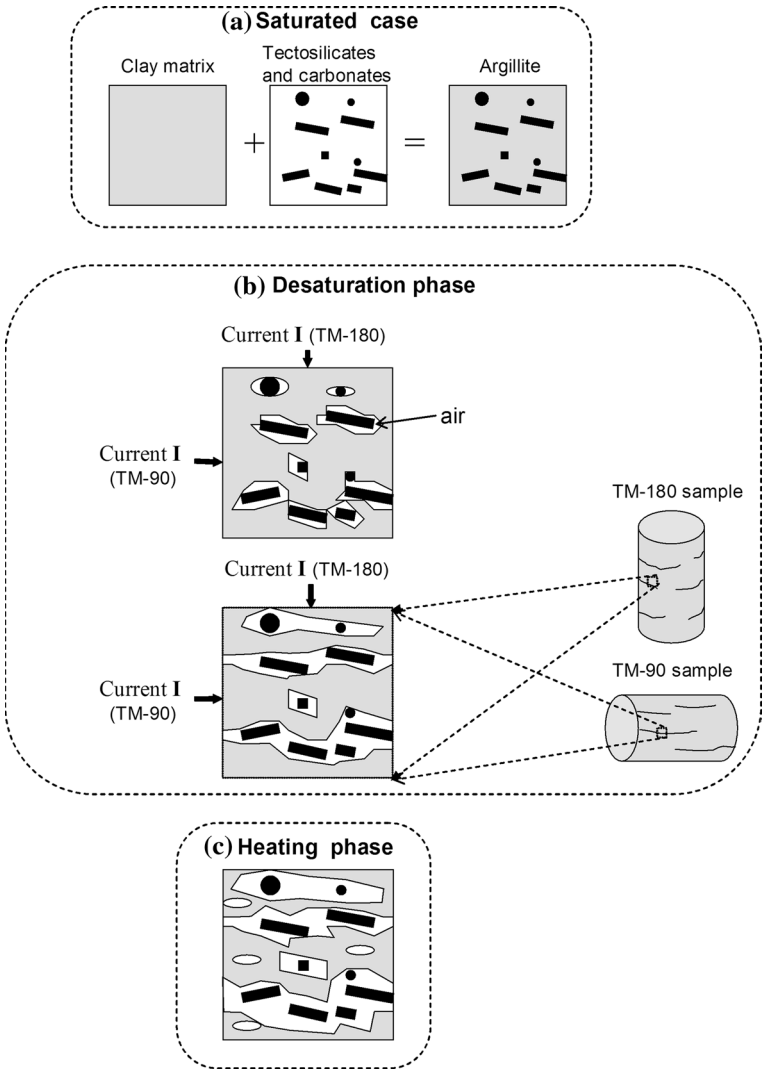

Figure 9
(a) Simplified texture of argillite in the saturated case (modified from SAMMARTINO *et al.*, 2003). (b) Textural evolution during the desaturation phase. In a first step, microcracks are generated from macropores mainly located at the clay-grain contacts, due to the shrinkage of the clay fraction. In a second step, these microcracks propagated subhorizontally into the anisotropic clay matrix. (c) Textural evolution during the heating phase (adapted from SAMMARTINO *et al.*, 2003).

few hundreds of micrometers), often aligned subhorizontally, i.e., perpendicular to the compaction and on the other hand, a fine and electrical-conducting fraction, i.e., the clay matrix in which clay particles (individual and/or aggregates of 2:1 illite, smectite or 1:1 kaolinite units) are also oriented perpendicularly to the compaction (e.g.,

DJÉRAN-MAIGRE *et al.*, 1998). Moreover, scanning electron microscope (SEM) images reveal that a major fraction of the macroporosity in argillite is located between the coarse phase and the clay matrix (SAMMARTINO *et al.,* 2003). This explains why voids and microcracks appear primarily around carbonates and quartz grains when a saturated argillite begins to dry (e.g., GASC-BARBIER *et al.*, 2000). As the desaturation process evolves, subhorizontal fractures parallel to the stratification are generated as a result of the coalescence of the initial voids and microcracks in the anisotropic clay matrix (Fig. 9B). Finally, the heating favours the occurrence of additional cracks mainly associated with the clay matrix (Fig. 9C).

Consequently, following these simple ideas, the complex resistivity measured perpendicular to the stratification (TM180 samples) and thus perpendicular to the desiccation-induced fractures is mainly affected by the nonconductive barriers constituting these microcracks. The current flow has to face the fractures directly. As a result, the microfractures which appear in the clay matrix during the heating phase have slightly more influence. Conversely, the complex resistivity measured parallel to the stratification (TM90 samples) is less influenced by the desiccation-induced microfractures generated during the desaturation phase since the latter are subparallel to the direction of the current flow. Measurements for TM90 samples will be more sensitive to microcracks in the clay matrix. This explains why a clear discontinuity in the evolution of SIP parameters is observed in Figures 5a, 5b, 8a, and 8b at the desaturation/heating transition.

5. Representation of Polarization Spectra

5.1. Conventional Empirical Models

In this section, the conventional empirical models widely used in IP studies are presented. Our objective is twofold: (1) To invert the data with these conventional models and (2) to provide a practical model (i.e., with the smallest number of independent parameters) to characterize the SIP spectra of clayey rocks undergoing drying.

The most popular empirical model is probably the Cole-Cole (CC) model (e.g., COLE and COLE, 1941; PELTON *et al.*, 1983; VANHALA, 1997):

$$\rho^*(\omega) = \rho_0 \left\{ 1 - m \left[1 - \frac{1}{1 + (i\omega\tau)^c} \right] \right\}, \tag{5}$$

where ρ_0 is the direct-current resistivity ($\Omega \cdot$ m) (i.e., $\rho \rightarrow \rho_0$ when $\omega \rightarrow 0$), m is the chargeability, c is the Cole-Cole exponent, τ is a time constant (s); ω is the angular frequency (rad/s) and $I^2 = -1$. The chargeability m describes the magnitude of the polarization effect while τ is related to the position of the phase peak, f_c, at which the phase reaches a maximum (PELTON *et al.*, 1983). This critical frequency is given by

$$f_c = \frac{1}{2\pi\tau(1-m)^{1/2c}}. \tag{6}$$

In order to represent simply their data, COLE and COLE (1941) chose to represent the real part $\mathrm{Re}(\rho^*)$ or ρ' and the imaginary part $\mathrm{Im}(\rho^*)$ or ρ'' of the measured complex resistivity ρ^* at each function, by points in the complex plane. This synthetic way to display dielectric data is now extensively used and examples are given in Figure 9. With this method of representation, called hereafter Argand representation, the CC model appears as a circular arc with its center either on or below the real axis of the complex plane (Fig. 10).

However, experimental investigations on rock samples have shown in several cases (porphyry copper deposits, some sedimentary rocks) that complex resistivity data could appear as a straight line in the Argan plane (VAN VOORHIS *et al.*, 1973; WELLER *et al.*, 1996): The real and imaginary parts obey identical power laws of frequency. Such data are represented in the so-called Drake model, also called the Constant-Phase-Angle (CPA) model. It can be expressed by the equation:

$$\rho^*(\omega) = \rho_0\left\{\frac{1}{(1+i\omega\tau)^a}\right\}, \tag{7}$$

where only three parameters ρ_0, τ and a are unknown. At high frequencies ($\omega\tau \gg 1$), the amplitude is given by

$$|\rho^*(\omega)| = \rho_0(\omega)^{-a}, \tag{8}$$

and the phase is given by:

$$\varphi = \frac{\pi}{2}a. \tag{9}$$

In order to model an asymmetrical circular arc in the Cole-Cole representation, the Cole-Davidson (CD) model has been proposed by DAVIDSON and COLE (1950) (Fig. 10):

$$\rho^*(\omega) = \rho_0\left\{1 - m\left[1 - \frac{1}{(1+i\omega\tau)^a}\right]\right\}. \tag{10}$$

The CC, CPA, and DC models also can be generalized into a single formulation; the so-called generalized, GCC model (PELTON *et al.*, 1983)

$$\rho^*(\omega) = \rho_0\left\{1 - m\left[1 - \frac{1}{(1+(i\omega\tau)^c)^a}\right]\right\}. \tag{11}$$

When $a = 1$ or $c = 1$, one obtains the CC model or the CD model, respectively. When $c = 1$ and $m = 1$, the CPA model is obtained. KLEIN and SILL (1982) showed that the GCC model is the best model to fit the experimental data obtained from artificial clay-bearing sandstones.

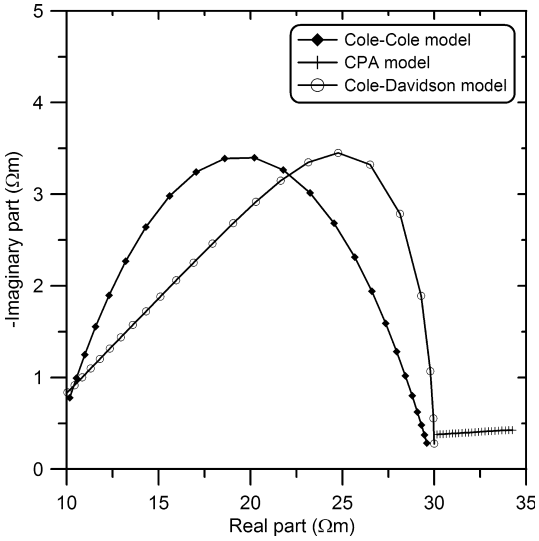

Figure 10
Examples of conventional empirical models displayed in an Argand representation: Cole-Cole model (with $\rho_0 = 30$ Ω.m, $\tau = 10^{-2}$ s, $m = 0.7$, $c = 0.4$); CPA model (with $\rho_0 = 35.5$ Ω.m, $\tau = 105$ s, $c = 0.008$), Davidson-Cole model $\rho_0 = 30$ Ω.m, $\tau = 10$ s, $m = 0.8$, $c = 0.13$).

5.2. Inversions of the Dielectric Spectra

The dielectric spectra have been inverted using a nonlinear iterative least-squares method (TARANTOLA and VALETTE, 1982) on the basis of the three representation models given above.

With respect to the desaturation phase, the inversion of the spectra of the TM90 samples shows that the CC formulation provides the best agreement when the chargeability is fixed equal to 1 (Fig. 11). The inversions of TM180 spectra were *a priori* more complex: As it is shown for the example given in Figure 11 (TM180-1424, w = 3.49%), these spectra indicate a linear element at the lowest part of the frequency range (0.18 Hz–5.86 Hz), i.e., with a frequency behavior corresponding to the power–law given by equation (8) ($\propto \omega^{-a}$). Consequently, the most suitable model for the TM180 samples is likely a combination of the CC model (for the high part of the frequency range) and the CPA model (for the low part of the frequency range).

Figure 12 illustrates the inversions corresponding to the data of the heating phase. The best agreement with the dielectric spectra was obtained with the GCC model which can reproduce the specific asymmetrical arcs observed in the Argand diagram of the complex resistivity (Fig. 12). For both desiccation phases, the evolutions of CC and GCC parameters as a function of the water content are given in Figures 13a, b, c, d and e. In these figures, the TM180 samples are not considered in the desaturation phase since their spectra could not be modelled by a single CC model.

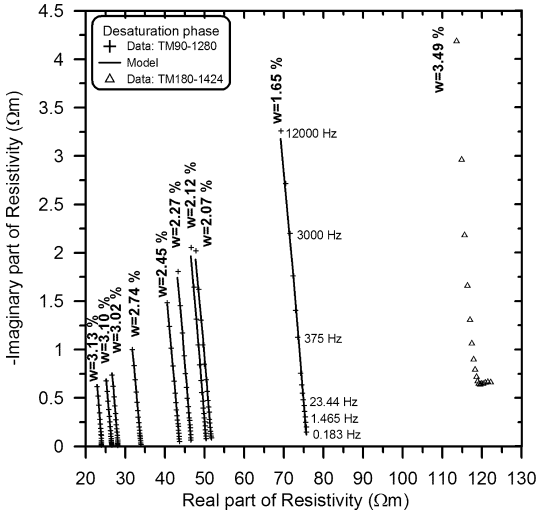

Figure 11
Examples of experimental and modelled dielectric spectra obtained during the desaturation phase in an Argand diagram.

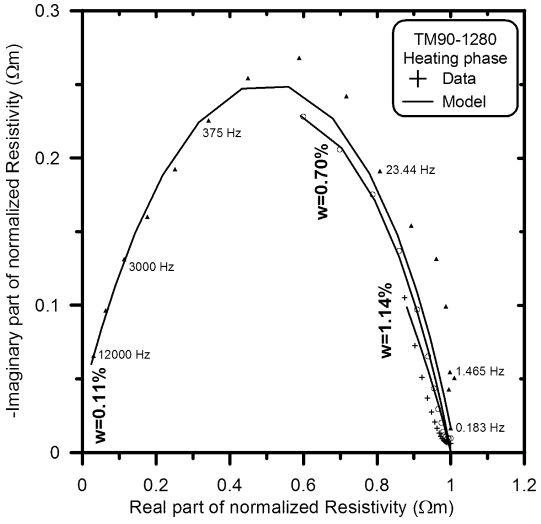

Figure 12
Experimental and modelled dielectric spectra of TM90-1280 samples obtained during the heating phase in an Argand diagram. The real and imaginary parts are normalized by the greatest value taken in each spectrum.

Figures 13a and 13d show that the parameters ρ_0 and τ are very sensitive to changes in the water content. The water content dependence of ρ_0 is not surprising since DC-resistivity is known to be a good indirect predictor of water content (e.g.,

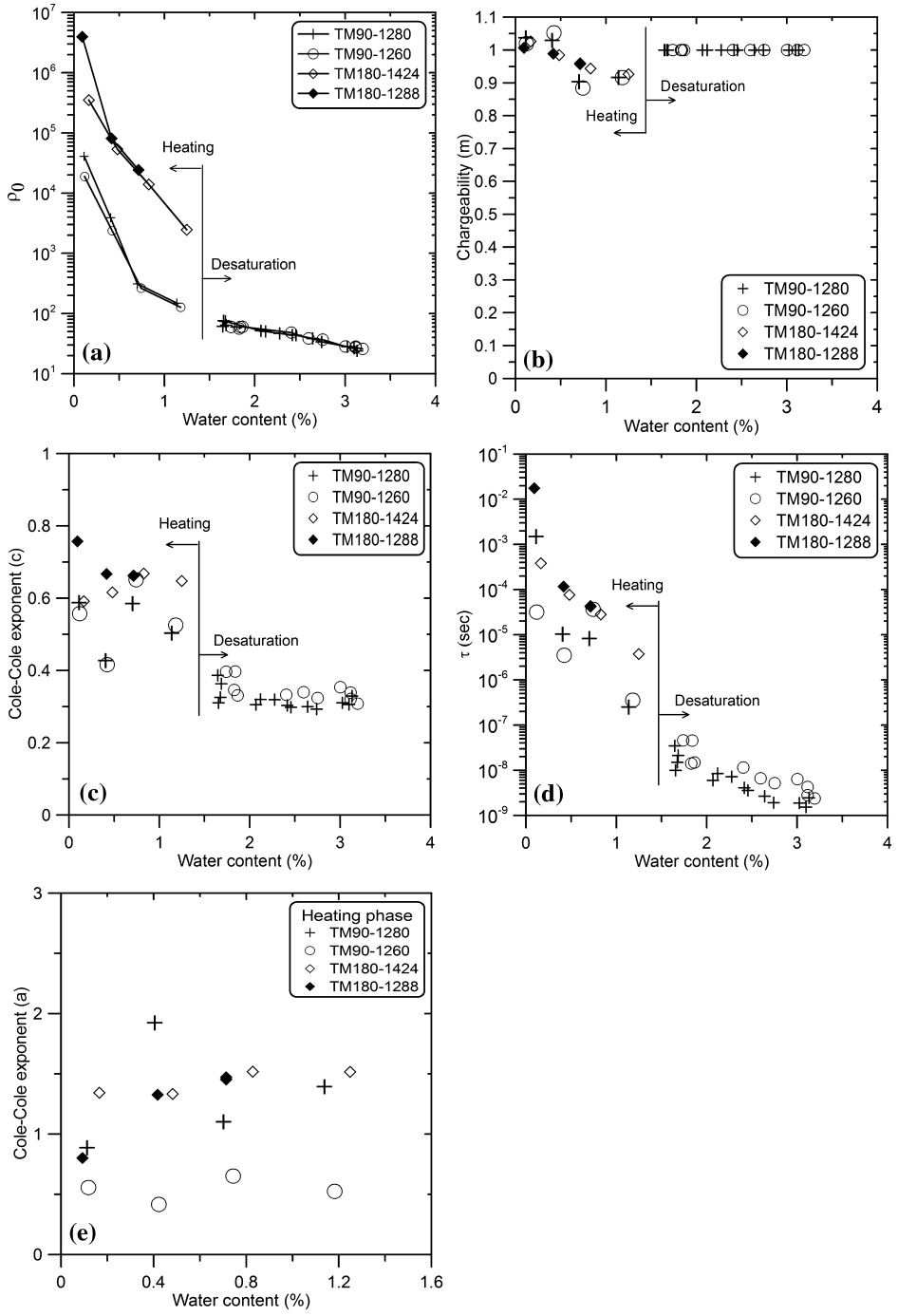

Figure 13
Inverted parameters of the Cole-Cole model and the Generalized Cole-Cole model as a function of water content. (a): The DC-resistivity ρ_0. (b) The chargeability m. (c) The Cole-Cole exponent c; (d) The time constant τ. (e) The exponent a of the Generalized Cole-Cole model.

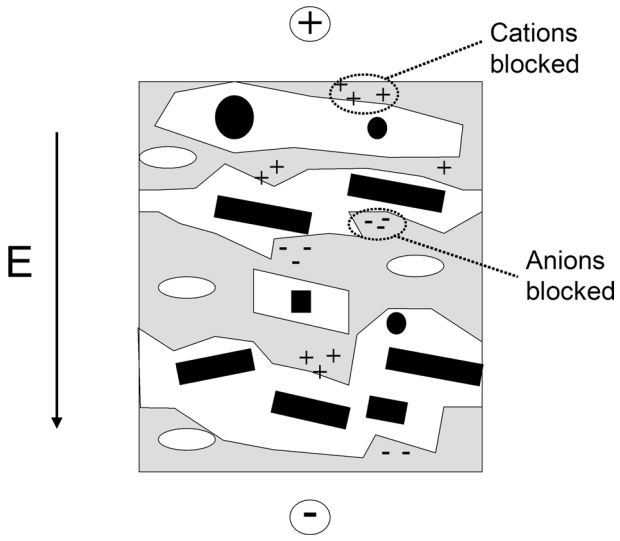

Figure 14
Schematic representation of the polarization process during the heating phase.

DANNOWSKI and YARAMANCI, 1999). However, the water content dependence of τ is more difficult to explain. This parameter is often linked to the size of polarizable grains (e.g., VANHALA, 1997). Nevertheless, when clay-bearing sedimentary rocks are considered, various formulations (e.g., MADDEN and MARSHALL, 1959; VINEGAR and WAXMAN, 1984; TITOV *et al.*, 2002, 2004) agree with the fact that the relaxation time τ depends on a characteristic length l between two selective zones following:

$$\tau \propto l^2. \tag{11}$$

In shaly sands, a selective zone, which corresponds to an accumulation of electrical charges (i.e., electrical poles) is typically an aggregate of clay minerals or the contact between two adjacent quartz grains coated by clay particles. This relationship $\tau(l)$ explains also why KLEIN and SILL (1982) found a good correlation between τ values inverted by a GCC model and the size of isolating beads in their artificial clay-glass beads mixtures.

We suggest that our τ values confirm these previous theoretical and experimental studies. As the heating occurs, the average distance between selective zones consisting of interfaces between shrunk clay matrix and some microcraks, increases due to the growth of the microcracks and the generation of new microcracks in the medium (Fig. 14). The corresponding electrical tortuosity increases. As a result, the parameter τ evolves drastically over five decades following a power-law as given in (11). This process is likely associated with the generation of new selective zones (i.e.,

new electrical poles). This is confirmed by the increase of the chargeability, m with the heating (Fig. 13b).

6. Conclusions

Low-frequency dielectric spectra measurements have been conducted on a set of argillite samples taken from the Tournemire test site, which is under study by the IRSN. The dielectric spectra have been recorded with samples submitted to the following desiccation path: (a) A desaturation phase under ambient air and then (b) a heating phase corresponding to four temperature levels (70°C, 80°C, 90°C, and 105°C).

This experimental investigation demonstrates (a) the interest of using the SIP method to remotely monitor both the water content and the thermally-induced microcracks and (b) that the best models to invert the dielectric spectra are the CC model and the GCC model for the desaturation phase and the heating phase, respectively. However, the data show that the development of the anisotropy can induce different spectral signatures and polarization processes. This may lead to difficulty for the use of a comprehensive model. In this situation a complex resistivity tensor should be introduced depending on the fabric tensor of the medium.

The next steps of this work would be (1) to improve our knowledge of the underlying physical process involved in the IP effect of clayey rocks and (2) to apply the SIP method in the field, i.e., in the gallery of a deep repository. Following the first task, as mentioned, the involved physical and chemical processes are complex and numerous: the membrane polarization effect, the Maxwell-Wagner effect, the polarization of the Electrical Double Layer. In our opinion, the best way to successfully reach this objective would be to use upscaling approaches associated with well-characterized physical processes previously identified by relevant microscopic observations (SEM, etc.).

Acknowledgements

This research was supported by the Agence Nationale de la Recherche (ANR) – ECCO program (POLARIS Project: ''Polarisation provoquée spectrale'' – Spectral-Induced Polarization). The authors thank Jean-Claude Gros, Justo Cabrera, and Karin Ben-Slimane of the French Institute for Radioprotection and Nuclear Safety (IRSN) for providing the argillite samples from the Tournemire site. We thank also Elizabeth Bemer and Jean-François Nauroy of the French Petroleum Institute (IFP) for providing the limestone samples.

References

ANDRA (Agence Nationale de Gestion des déchets Radioactifs) (2005a), Dossier 2005, *Argile – Synthèse – Evaluation de la Faisabilité du Stockage Géologique en Formation Argileuse,* ANDRA Report n° C RP ADP 04-0002.

ANDRA (Agence Nationale de Gestion des déchets Radioactifs) (2005b), Dossier 2005, *Argile – Référentiel du site de Meuse/Haute-Marne, Tome 2: Caractérisation Comportementale du Milieu Géologique sous Perturbation,*ANDRA Report n° C RP ADP 04-0022.A.

Bemer, E., Vincké, O., and Loguemare, P. (2004), *Geomechanical log deduced from porosity and mineralogical content*, Oil and Gas Sci. and Tech. *59*, 4, 405–406.

Bérest, P. and Weber, Ph., *La Thermomécanique des Roches* (BRGM, Orléans, 1988).

Binley, A., Slater, L. D., Fukes, M., and Cassiani, G. (2005), *Relationship between Spectral-Induced Polarization and Hydraulic Properties of Saturated and Unsaturated Sandstone*, Water Resour. Res. *41*, 12, W12417, doi: 10.1029/2005WR004202.

Bonin, B. (1998), *Deep geological disposal in argillaceous formations: Studies at the Tournemire Test Site*, J. Contam. Hydrol. *35*, 315–330.

Cabrera, J., Beaucaire, C., Bruno, G., de Windt, L., Genty, A., Ramambasoa, N., Rejeb, A., Savoye, S., and Volant, P. (2001), *Projet Tournemire: Synthèse des Résultats des Programmes de Recherche 1995/1999*. IRSN Report.

Charpentier, D., Tessier, D., and Cathelineau, M. (2003), *Shale microstructure evolution due to tunnel excavation after 100 years and impact of tectonic paleofracturing*. Case of Tournemire, France., Eng. Geol. *70*, 55–69.

Carrier, M. and Soga, K. (1999), *A four terminal measurement system for measuring the dielectric properties of clay at low frequency*, Eng. Geol. *53*, 2, 115–123.

Charpentier, D., Mosser-Ruck, R., Cathelineau, M., and Guillaume, D. (2004), *Oxidation of Mudstone in a Tunnel (Tournemire, France): Consequences for the Mineralogy and Chemistry of Clays Minerals*, Clay Minerals *39*, 135–149.

Chelidze, T. L., Guéguen, Y., and Ruffet, C. (1999), *Electrical spectroscopy of porous rocks: A review – II. Experimental results and interpretation*, Geophys. J. Int. *137*, 16–34.

Cole, K. S. and Cole, R. H. (1941), *Dispersion and absorption in dielectrics,* J. Chem. Phys. *9*, 341–351.

Cosenza, P., Ghoreychi, M., de Marsily, G., Vasseur, G., and Violette, S. (2002), *theoretical prediction of poroelastic properties of Argillaceous rocks from in situ specific storage coefficient*, Water Resour. Res. *38*, 10, 1207, doi: 10.1029/2001WR001201.

Dannowski, G. and Yaramanci, U. (1999), *Estimation of water content and porosity using combined radar and geoelectrical measurements*, European J. Env. and Eng. Geophys. *4*, 71–85.

Davidson, D. W. and Cole, R. H. (1950), *Dielectric relaxation in glycerine*, J. Chem. Phys. 18, 1417.

de Windt, L., Cabrera, J., and Boisson, J.-Y., *Hydrochemistry in an Indurated Argillaceous Formation (Tournemire Tunnel Site, France)*. In *Water-Rock Interaction* (eds. Arehart and Hulston), (Balkema, Rotterdam, 1998) pp. 145–148.

Devivier, K., Devol-Brown, I., and Savoye, S. (2004), *Study of iodide sorption to the Argillite of Tournemire in Alkaline media*, Appl. Clay Sci. *26*, 171–179.

Djéran-maigre, I., Tessier, D., Grunberger, D., Velde, B., and Vasseur, G. (1998), *Evolution of microstructures and of macroscopic properties of some clays during experimental compaction,* Marine and Petroleum Geology *15*, 109–128.

Dukhin, S.S. and Shilov, V.N., *Dielectric Phenomena and the Double Layer in Disperse Systems and Polyelectrolytes* (Wiley, New York 1974).

Gasc-Barbier, M., Cosenza, P., Ghoreychi, M., and Chanchole, S., *Laboratory Experiments on Swelling-Shrinkage of Deep Clay under Triaxial Tests*, Eurock2000 Symp. Aachen, Germany, 27–31 March, (ed. Verlag Glükauf, Essen 2000).

Garrouch, A. A. and Sharma, M. M. (1994), *The influence of clay content, salinity, stress, and wettability on the dielectric properties of brine saturated rocks: 10 hz to 10 mhz*, Geophysics *59*, 6, 909–917.

GLOVER, P. W., GOMEZ, J. B., MEREDITH, P. G., HAYASHI, K. P. R., SAMMONDS, and MURRELL, S. A. F. (1997), *Damage of saturated rocks undergoing triaxial deformation using complex electrical conductivity measurements: Experimental results*, Phys. Chem. Earth. *22*, 1–2, 57–61.

GLOVER, P. W., GOMEZ, J. B., and MEREDITH, P. G. (2000), *Fracturating in saturated rocks undergoing triaxial deformation using complex electrical conductivity measurements: Experimental study*, Earth Planet. Sci. Lett. *5621*, 201–213.

HEIKAMP, S., and NOVER, G. (2003), *An integrated study on physical properties of a KTB gneiss sample and marble from Portugal: Pressure dependence of the permeability and frequency dependence of the complex electrical impedance*, Pure Appl. Geophys. *160*, 929–936.

KALUZNY, Y., *Evaluation de la Sûreté du Stockage de Déchets Radioactifs en Formation Géologique Profonde*. In *Stockage en souterrain* (ed. G. Rousset) (Presses des Ponts et Chaussées, Paris, 1990) pp. 265–276.

KLEIN, J. D. and SILL, W. R. (1982), *Electrical properties of Artificial clay-bearing sandstone*, Geophys. *47*, 11, 1593–1605.

KRUSCHWITZ, S. and YARAMANCI, U. (2004), *Detection and characterization of the disturbed rock zone in claystone with complex resistivity method*, J. Appl. Geophys. *57*, 63–79.

LEVITSKAYA, T. M. and STENBERG, B. K. (1996), *Polarization processes in rocks 2. Complex dielectric permittivity method,* Radio Sci. *4*, 781–802.

MARSHALL, D. J. and MADDEN, T. R. (1959), *Induced polarization: A study of its causes*, Geophys. *24*, 790–816.

MITCHELL, J. K., *Fundamentals of Soils Behavior* (Wiley, New York 1973).

NIANDOU, H., SHAO, J. F., HENRY, J.-P., and FOURMAINTRAUX, D. (1997), *Laboratory investigation of the mechanical behaviour of Tournemire shale*, Int. J. Rock Mech. Min. Sci. *34*, 3–16.

NOVER, G., HEIKAMP, S., and FREUND, D. (2000), *Electrical impedance spectroscopy used as a tool for the detection of fractures in rock samples exposed to either hydrostatic or triaxial pressure conditions,* Natural Hazards *21*, 317–330.

OLHOEFT, G. (1985), *Low-frequency electrical properties*, Geophys. *50*, 2492–2503.

PELTON, W. H., SILL, W. R., and SMITH, B. D. (1983), *Interpretation of complex resistivity and dielectric data, Part I.*, Geophys. Trans. *29*, 4, 297–330.

REVIL, A. L. M., CATHLES, III, LOSH, S., and NUNN, J. A. (1998), *Electrical conductivity in shaly sands with geophysical applications,* J. Geophys. Res. *103*(B3), 925–936.

ROUSSET, G. (1988), *Comportement Mécanique des Argiles Profondes, Application au Stockagede DéchetsRadioactifs*, Ph.D. Dissertation, Paris, Ecole Nationale des Ponts et Chaussées.

SAMMARTINO, S., BOUCHET, A., PRÊT, D., PARNEIX, J.-C., and TEVISSEN, E. (2003), *Spatial distribution of porosity and minerals in clay rocks from the Callovo-Oxfordian formation (Meuse-Haute-Marne, Eastern France) – Implications on ionic species diffusion and rock sorption capability*, Appl. Clay Sci. 157–166.

TARANTOLA, A. and VALETTE, B. (1982), *Generalized Non linear inverse problem solved using the least square criterion*, Rev. Geophys. Space Phys. *20*(2), 219–232.

TESSIER, D. (1987), *Etude de l'Organisation des Argiles Calciques. Evolution au cours de la dessiccation*, Ann. Agro. *29*, 4, 319–355.

TITOV, K., KOMAROV, V., TARASOV, V., and LEVITSKI, A. (2002), *Theoretical and experimental study of time-domain-induced polarization in water saturated sands*, J. Appl. Geophys. *50*, 4, 417–433.

TITOV, K., KEMNA, A., TARASOV, A., and VEREECKEN, H. (2004), *Induced polarization of unsaturated sands determined through time domain measurements*, Vadose Zone J. *3*, 1160–1168.

VALÈS, F., NGUYEN MINH, D., GHARBI, H., and REJEB, A. (2004), *Experimental study of the influence of the degree of saturation on physical and mechanical properties in Tournemire shale (France)*, Appl. Clay Sci. *26*, 197–207.

VAN VOORHIS, G. D., NELSON, P. H., and DRAKE, T. L. (1973), *Complex resistivity spectra of porphyry cooper mineralization*, Geophys. *38*, 49–60.

VANHALA, H. and SOININEN, H. (1995), *Laboratory technique for measurement of spectral induced polarization response of soil samples*, Geophys. Prospecting *43*, 655–676.

VANHALA, H. (1997), *Laboratory and Field Studies of Environmental and Exploration Applications of the Spectral Induced Polarization (SIP) Method*, Ph.D. Dissertation, Helsinki University of Technology.

VINEGAR, H. J. and WAXMAN, M. H. (1984), *Induced polarization of shaly sands*, Geophys. *49*, 9, 1267–1287.

WELLER, A., SEICHTER, M., and KAMPKE, A. (1996), *Induced-polarization modelling using complex conductivities*, Geophys. J. Intern. *127*, 387–398.

(Received March 31, 2006, accepted January 31, 2007)